Journal of Thermal Analysis and Calorimetry (2023) 148:2265–2271
https://doi.org/10.1007/s10973-022-11913-4

Thermodynamic heat-transfer phenomena in nanostructured glassy substances: a comparative study on g-As_5Se_{95} and g-$As_{55}Se_{45}$

Andrzej Kozdras[1] · Oleh Shpotyuk[2,3] · Bohdan Mahlovanyi[4,5] · Yaroslav Shpotyuk[4,5] · Andriy Kovalskiy[6]

Received: 15 January 2022 / Accepted: 19 December 2022 / Published online: 5 January 2023

Abstract
Nanostructurization-driven responses in calorimetric heat-transfer phenomena are compared for glassy arsenoselenides at different levels of their molecular network organization, namely in high-polymerized g-As_5Se_{95} and low-polymerized g-$As_{55}Se_{45}$, employing multifrequency temperature-modulated DSC-TOPEM® method complemented with Raman scattering microspectroscopy. It is shown that high-polymerized network composed of $AsSe_3$ pyramids interlinked by Se chains with small number of Se_8 molecular units decoupled from this network prevails in melt-quenched and nanomilling-derived g-As_5Se_{95}. Transition to more polymerized network due to incorporation of destroyed Se_8 molecules into glass backbone occurs in this glass under nanostructurization. As a result, nanostructurization-driven calorimetric response in g-As_5Se_{95} dominates by size-induced glass-transition temperature depression. The low-polymerized structure of g-$As_{55}Se_{45}$ is built of As–Se network enriched with tetra-arsenic selenide molecular units decoupled from this network. Molecular-to-network transition owing to nanomilling-driven destruction of these cage molecules and their incorporation into newly polymerized glass-forming backbone occurs in g-$As_{55}Se_{45}$ resulting in strong increase in calorimetric glass-transition temperature.

Keyword DSC · Heat transfer · Multiphase · Nanostructure

Background

Nanostructured materials are distinguished by great variety of *size-dependent phenomena* which play a pivotal role in the majority of their practical applications [1]. Thus, being transferred to a nanoscale level evolving agglomerates of atoms and/or atomic groups composing nanoparticles, these nanoscopic materials demonstrate strong propensity to *multiphase* occurrence, modifying essentially calorimetric responses from conventional *heat-transfer phenomena* [1–3]. As a rule, clear *reduction* trend dominates in characteristic *interphase transition* temperatures in nanostructured crystalline materials below some *critical nanosizes*, when one of the metastable phases becomes thermodynamically more favorable over others [3–7].

The similar trend is character for amorphous polymeric substances, which typically reveal notable *depression* trend in glass-transition temperature T_g when being prepared as thin and ultra-thin (having a few nm in thickness) films [8–12].

However, in some amorphous materials belonging to molecular network chalcogenide glass-formers [13, 14] such as melt-quenched glassy arsenoselenides g-As-Se possessing structural conformations with different degrees of polymerization [15, 16], the calorimetric response on transferring to nanoscale is expected to be more complicated because of possible effect from nanostructurization-driven *molecular-to-network* transitions (as was also in the case of isotypical glassy arsenosulphides g-As–S [17, 18]). Stable low-polymerized (preferentially molecular-type) and high-polymerized (preferentially network-type) atomistic structures in

✉ Oleh Shpotyuk
olehshpotyuk@yahoo.com

1 Opole University of Technology, 75, Ozimska Str., 45370 Opole, Poland

2 Jan Dlugosz University in Czestochowa, 13/15, Al. Armii Krajowej, 42201 Czestochowa, Poland

3 O.G. Vlokh Institute of Physical Optics, 23, Dragomanov Str., Lviv 79005, Ukraine

4 Institute of Physics, University of Rzeszow, 1, Pigonia Str., 35-959 Rzeszow, Poland

5 Ivan Franko National University of Lviv, 107, Tarnavskogo Str., Lviv 79017, Ukraine

6 Austin Peay State University, Clarksville, TN 37044, USA

g-As–Se subjected to nanostructurization through high-energy mechanical milling were refined with a help of X-ray powder diffraction (XRPD) analysis [19]. It was shown that cage-like molecular entities stabilized initially in melt-quenched g-As–Se were merely destroyed under high-energy mechanical milling-driven nanostructurization facilitating formation of more polymerized chain-like network structures, this process being referred to as re-amorphization [20]. The objective of the current research is to compare most plausible nanostructurization-driven responses in the glass-transition region of these arsenoselenide glasses revealed at principally different levels of their molecular network arrangement, namely in high-polymerized g-As_5Se_{95} and low-polymerized g-$As_{55}Se_{45}$ specimens, employing the multifrequency temperature-modulated DSC-TOPEM® method complemented with microstructural characterization using the Raman scattering (RS) microspectroscopy.

Materials and methods

The bulk samples of glassy g-As_5S_{95} and g-$As_{55}S_{45}$ were prepared from high-purity elemental precursors (As and Se of 5 N purity) employing conventional *melt quenching* technological route, that is rapid cooling of the glass from melt-liquid state [13]. The melt-rocking operation was used to prepare homogeneous alloys (as was justified by Lucas et al. [21]), avoiding necessity of extra-long homogenization stabilizing these glasses from very unfavorable vertical position in the furnace [22]. The sealed ampoules with elemental precursors taken in the ratio corresponding to As_5S_{95} and $As_{55}S_{45}$ compositions were heated in a rocking furnace up to 650 °C in 6 h and then homogenized at this temperature for 10 h. At the finishing stage, the ampoule was cooled down to 500 °C and finally quenched in a water. To eliminate mechanical strains appeared in bulky material after rapid cooling, the just-synthesized glasses were annealed at 120 °C for 1 h. The ingots extracted from ampoules were amorphous, as it followed from the XRPD analysis, conch-like fracture and IR transparency of freshly prepared cut sections. The room temperature densities of g-As_5S_{95} and g-$As_{55}S_{45}$ samples determined by the Archimedes displacement in ethanol using the Mettler Toledo balances were (4.310 ± 0.005) g cm^{-3} and (4.447 ± 0.005) g cm^{-3}, respectively, in full agreement with the known atomic densities of compositionally similar glassy counterparts from binary As-Se system [15, 16].

The melt-quenched bulk chalcogenide glasses of the above chemical compositions (hereafter referred to as *unmilled* samples) were subjected to nanostructurization by *high-energy mechanical milling* (nanomilling) in a dry mode using Pulverisette 6 mill operated at protective Ar atmosphere and 500 min^{-1} rotational speed. This procedure was performed for 60 min in 250 mL tungsten carbide chamber loaded with 50 balls (each having 10 mm in diameter), using ~ 3 g of coarse-grained glass sieved under 200 µm. The amorphous state of the samples was not changed under nanomilling, as it follows from diffuse peak-halos in their XRPD patterns [19, 20]. The fine-grained powdered substance was finally compressed in stainless steel die (under ~ 0.7 GPa) to produce the disc-like pellets (having ~ 6 mm in diameter and ~ 1 mm in thickness) most suitable for further microstructural characterization research.

Calorimetric thermo-analytical measurements were performed employing multifrequency temperature-modulated DSC-TOPEM® with DSC-1 calorimeter (Mettler Toledo, Switzerland), as described in more details elsewhere [17, 18]. In this method, stochastic temperature modulations are superimposed on underlying rate of DSC scans, resulting in frequency dependent and independent phenomena [23]. This provides more information on thermodynamic stability of the revealed phases. The DSC-TOPEM® instrument was equipped with FRS5 + sensor and HT100 (Huber, Germany) intracooler, the STAR^e ver. 13a software being used to control experimental conditions and process the data. The calorimeter was multi-point calibrated using In and Zn standard probes. The tested samples (ca. 10–15.0) were encapsulated in sealed 20 µL Al pans kept in protective N_2 atmosphere, and scanned at the rate of 1.0 K min^{-1} stochastically modulated in pulses between 15 and 40 s, the pulse height being 1 K. The evaluations were adjusted using sapphire reference curve, the width and shift of calculation window being 60 s and 1 s, respectively.

The detected calorimetric events were parameterized using the DSC-TOPEM® profiles presenting temperature variations of non-reversing (HF_{nrev}) and reversing (HF_{rev}) heat flow in the heating run, each measuring protocol being averaged in triplicate. The reversing thermal effects, resulted from second-order phase transitions such as glass transition [24], were parameterized by heat capacity step-like jump (ΔC_p) allowing characteristic glass-transition temperatures determination in onset (T_g^{onset}) and mid-point (T_g^{mid}) presentation [24, 25]. The non-reversing thermal effects, connected with enthalpy relaxation in the glass-transition region during heating run, were parameterized by specific enthalpies difference ΔH [17, 25].

Microstructural nature of nanostructurization-driven transformations in the glass was identified with *micro-Raman spectroscopy* using the Horiba Xplora spectrometer equipped by CCD detector operated at room temperature. The CW 785 nm laser of 90 mW output power was employed for excitation, the 10% power option being used to avoid photostructural effects. Other measurement options applied were as follows: × 100 objective, 1800 1 mm^{-1} grating, 500 µm hole, and 50 µm slit. The spectral resolution was maintained at around 2 cm^{-1} and spatial resolution was near

2 μm. A number of scans were chosen in dependence on the surface of pelletized glass samples. Numerous scans on the entire surface were performed to be sure that RS spectra processed with the Horiba LabSpec software were reasonably identical. The milled and unmilled samples were compared through normalization by matching spectral areas in the region of interest. The detected RS bands were identified using the known data for numerous glassy analogs [26, 27].

Results and discussion

Thermodynamic heat-transfer responses were detected in the pellets of arsenoselenide glasses by multifrequency DSC-TOPEM® method. The temperature-modulated DSC-TOPEM profiles showing variation of reversing (HF_{rev}) and non-reversing (HF_{nrev}) heat flow in the bulky melt-quenched (unmilled) and nanostructurized (milled, viz. subjected to high-energy mechanical milling) g-As_5Se_{95} and g-$As_{55}Se_{45}$ samples are depicted on Figs. 1, 2, respectively, the calorimetric parameters derived from these curves being gathered in Table 1.

Under heating run, the principal endothermic thermal alteration event in the studied substance represents glass transition. In modulated DSC-TOPEM profiles of unmilled g-As_5Se_{95} sample depicted on Fig. 1a, the characteristic step-like jump supplemented by small peak is revealed in the temperature behavior of reversing (HF_{rev}) heat flow near the glass-transition region with heat capacity variation ΔC_p approaching ~ 0.14 J g^{-1} K^{-1}, while distinct peak with specific enthalpies difference of $\Delta H \sim 3.32$ J g^{-1} is observed in non-reversing (HF_{nrev}) heat flow dependence shown on Fig. 1b. The similar calorimetric thermal alteration responses are character for other families of chalcogenide glasses undergoing physical aging [28, 29].

An evident depression in the glass-transition temperature T_g is observed in modulated DSC-TOPEM profiles of this g-As_5Se_{95} sample after nanomilling, and this trend being accompanied by increase in the DSC-TOPEM peak amplitude. As it follows from Table 1, the T_g^{onset} value is reduced in milled g-As_5Se_{95} on 2.6 °C (from 69.3 to 66.7 °C), while specific enthalpies difference ΔH derived from temperature variation of non-reversing (HF_{nrev}) heat flow is enriched on more than 16% (reaching as high as 3.86 J g^{-1}). Noteworthy, the glass-transition width defined from temperature dependence of reversing (HF_{rev}) heat flow on Fig. 1a for g-As_5Se_{95} samples nanostructurized by high-energy mechanical milling does not change essentially.

Thus, milling-driven nanostructurization of chalcogenide glasses possessing highly polymerized network (such as under-stoichiometeric g-As_5Se_{95}) prevails by the known effect of size-induced glass-transition temperature T_g depression, which has been extensively studied from the mid 1990s

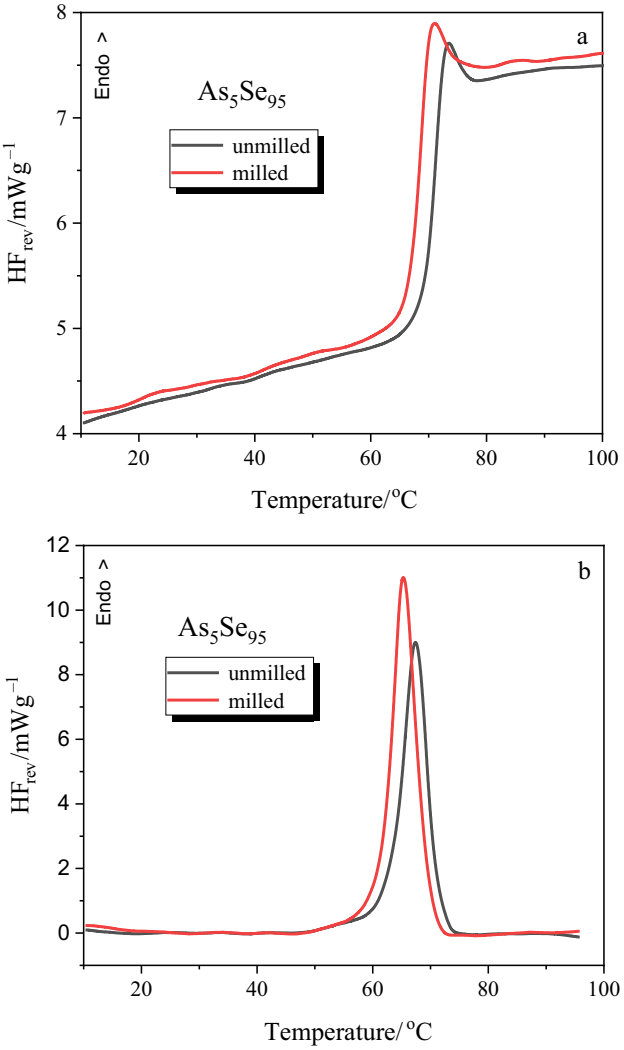

Fig. 1 Modulated DSC-TOPEM profiles showing temperature variation of reversing HF_{rev} (**a**) and non-reversing HF_{nrev} (**b**) heat flow in unmilled (black line) and milled (red line) g-As_5Se_{95}

[8–12]. However, this calorimetric heat-transfer phenomenon is cardinally changed in case of glasses having more irregular molecular-like structure (such as over-stoichiometric g-$As_{55}Se_{45}$). The bulk glass of this composition derived by melt quenching shows similar responses (albeit more reduced ones in modulated DSC-TOPEM profiles) within the glass-transition region, particularly, the characteristic step-like jump without accompanied peak in reversing (HF_{rev}) heat flow on Fig. 2a with $\Delta C_p \sim 0.11$ J g^{-1} K^{-1} (Table 1) and distinct endothermic peak in non-reversing (HF_{nrev}) heat flow on Fig. 2b with $\Delta H \sim 5.57$ J g^{-1}. The value of T_g^{onset} temperature for this unmilled glass (g-$As_{55}Se_{45}$) defined from reversing curve occurs to be 134.6 °C (Table 1), and this value being in an excellent agreement with reduced glass-transition temperatures in the As-rich arsenoselenide glasses

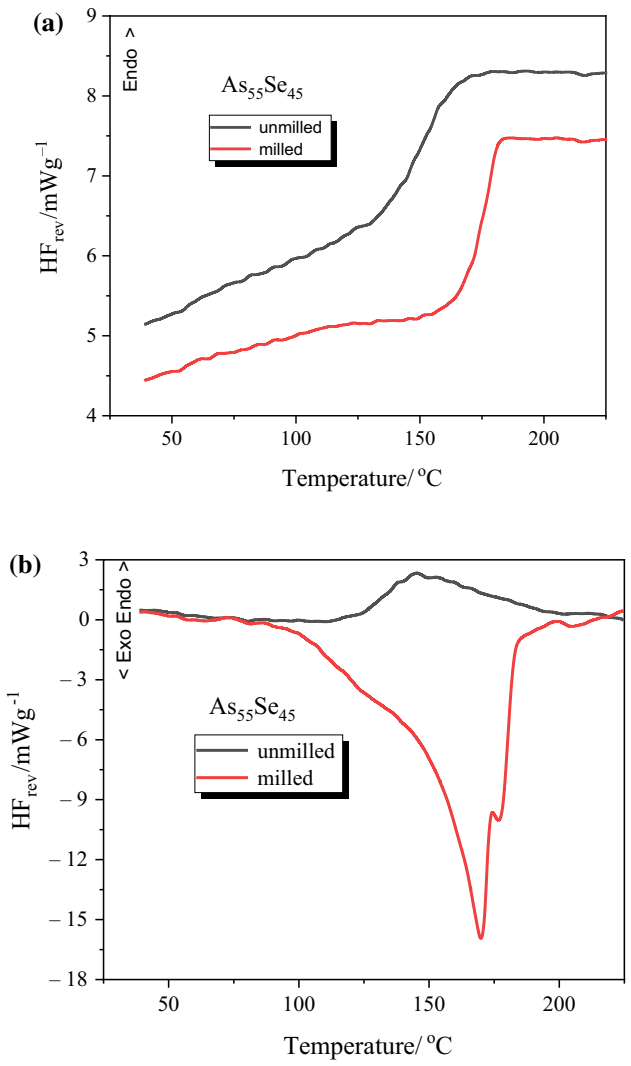

Fig. 2 Modulated DSC-TOPEM profiles showing temperature variation of reversing HF_{rev} (**a**) and non-reversing HF_{nrev} (**b**) heat flow in unmilled (black line) and milled (red line) g-$As_{55}Se_{45}$

ascribed to variance of different molecular tetra-arsenic selenide species (such as As_4Se_4, As_4Se_3, As_4) [16].

Under transition to more polymerized structure of g-$As_{55}Se_{45}$ samples undergoing nanomilling, the bulk glass-transition temperature notably increases approaching T_g^{onset} ~ 170.0 °C (see Table 1), the value character for unmilled melt-quenched samples of stoichiometric arsenic triselenide glass g-As_2Se_3 [15, 16]. At the same time, the glass-transition temperature width in nanomilled g-$As_{55}Se_{45}$ defined from reversing heat flow curve on Fig. 2a is narrowed by a factor at least 2.

The principal calorimetric response originated from non-reversing (HF_{nrev}) heat flow variation is changed drastically in nanostructurized g-$As_{55}Se_{45}$ due to thermal relaxation of strong inner strength generated in this glass under high-energy mechanical milling. As a result, the pronounced *exothermic* event (depicted on Fig. 2b) with specific enthalpies difference ΔH approaching as high as -29.70 J g^{-1} (see Table 1) prevails in this glassy sample (nanomilled g-$As_{55}Se_{45}$).

To shed light on the nature of *nanomilling-driven microstructural transformations* in the studied glasses, the micro-RS spectra were collected and compared for g-As_5Se_{95} and g-$As_{55}Se_{45}$ samples in both unmilled (melt-quenched) and milled (nanostructurized) states (Fig. 3, 4).

In the micro-RS-spectrum of melt-quenched g-As_5Se_{95} (Fig. 3, black curve) only a few bands are resolved, these being weak and relatively narrow band near ~ 107 cm^{-1} and ~ 132 cm^{-1}, weak but evidently broader band positioned near ~ 490 cm^{-1} and very strong band near ~ 248 cm^{-1}. The latter is due to overlapping of bond-stretching vibrational modes assigned to trigonal $AsSe_3$ pyramids at 227 cm^{-1} [30], and modes at ~ 230–270 cm^{-1} assigned to multiatomic Se fragments incorporated in various local environment [31], in part, strongly correlated chains disposed in trigonal t-Se conformations at 234 cm^{-1}, dissolved multi-Se chains at 250 cm^{-1} and molecular-type Se_8 species at ~ 260 cm^{-1}. The band at 107 cm^{-1} is probably connected with Se_8 rings contributing through A_1 mode at 112 cm^{-1} [32], while 132 cm^{-1} band is due to Se polymeric chains having RS-active E mode positioned at 138 cm^{-1} [32]. The broad RS-active band at 490 cm^{-1} is related to second-order Raman scattering from homonuclear Se-Se bonds [33]. Thus, the structure of unmilled g-As_5Se_{95} represents highly polymerized network built of $AsSe_3$ pyramids interlinked by Se chains with very small number of molecular units (such as Se_8) decoupled from this network.

Table 1 Parameterization of multifrequency temperature-modulated DSC-TOPEM profiles for melt-quenched bulk (unmilled) and nanostructurized (milled) glasses derived from reversing (HF_{rev}) and non-reversing (HF_{nrev}) heat flow variations

Glass samples		HF_{rev}			HF_{nrev}
		Glass-transition temperature		Heat capacity variation	Specific enthalpies difference
		T_g^{onset}/°C	T_g^{mid}/°C	ΔC_p/J g^{-1} K^{-1}	ΔH/J g^{-1}
g-As_5Se_{95}	Unmilled	69.3	70.7	0.14	3.32
	Milled	66.7	68.0	0.15	3.86
g-$As_{55}Se_{45}$	Unmilled	134.6	151.8	0.11	5.57
	Milled	170.0	174.6	0.13	– 29.70

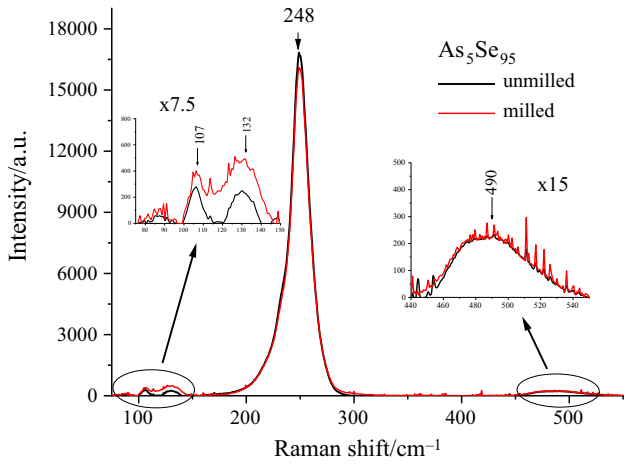

Fig. 3 Micro-RS spectra collected from unmilled (black curve) and milled (red curve) g-As_5Se_{95}. The most prominent RS-active bands are positioned by arrows. The insets represent enhanced RS bands in some spectral domains of interest (see text for more details)

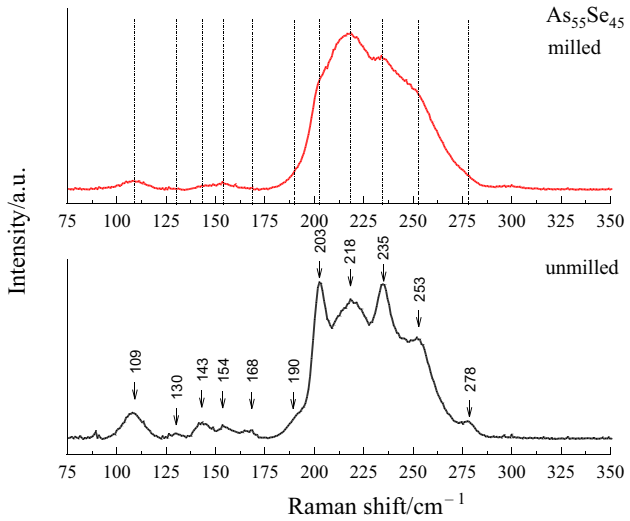

Fig. 4 Micro-RS spectra collected from unmilled (black curve) and milled (red curve) g-$As_{55}Se_{45}$. The most prominent RS-active modes in spectrum of bulk sample are positioned by arrows, and traced by dotted lines to micro-RS spectrum of nanostructured sample (see text for more details)

Only slight changes occur in the RS spectrum of this glass subjected to nanostructurization through milling (also shown on Fig. 3). The RS band at ~ 132 cm^{-1} ascribed to E mode of Se chains is increased in nanomilled g-As_5Se_{95}. Strong band at ~ 248 cm^{-1} does not change its position after nanomilling, while being slightly depressed, especially from the high-frequency side corresponding to spectral domain of preferential location of intramolecular bond-stretching modes ascribed to Se_8 molecules [31, 32]. Due to incorporation of atomic remainders of destroyed molecular units into glass network, the milled specimen becomes more polymerized, and this effect being associated with slight increase in the respective glass-transition parameters on this glass (see Table 1).

In the collected micro-RS-spectrum of melt-quenched g-$As_{55}Se_{45}$ depicted on Fig. 4, several low-frequency bands (at 109, 130, 143, 154, 168 and 190 cm^{-1}) and high-frequency bands (at 203, 218, 235, 253 and 278 cm^{-1}) are resolved. The high-frequency bands are ascribed to overlapped (preferentially strong) bond-stretching vibrational modes of $AsSe_3$ pyramidal units at 227 cm^{-1} [30], and some fingerprints of cage-like arsenoselenide molecules, such as As_4Se_4 at 248 and 190 cm^{-1} [34]; As_4Se_3 at 196, 242, 256, 266 and 280 cm^{-1} [35], as well as As_4 at ~ 200 cm^{-1} [33]. The low-frequency peaks (preferentially weak and medium) can be ascribed to bond-bending vibrational modes of these molecular cages, in part, As_4Se_3 at 140 and 166 cm^{-1} [26] and As_4Se_4 at 106, 136, 144, 190 and 207 cm^{-1} [34].

In the milled g-$As_{55}Se_{45}$ samples, all the above features observed in the micro-RS spectra are essentially broadened and depressed (see Fig. 1, red curve), testifying in favor of nanostructurization-driven destruction of respective tetra-arsenic selenide molecular units and their incorporation in newly polymerized arsenoselenide glass-forming network. Thus, the structure of this nanostructurized chalcogenide glass becomes notably stressed (as compared with iso-compositional unmilled sample), being affected by a variety of structural defects generated under high-energy mechanical milling. Atomic remainders of destroyed molecules are reincorporated into a glassy network, completely changing calorimetric response from the glass-transition event.

Conclusions

Nanostructurization-driven thermodynamic responses in calorimetric heat-transfer phenomena are compared for glassy arsenoselenides at principally different levels of their molecular network organization, namely in high-polymerized under-stoichiometric (preferentially network-type) g-As_5Se_{95} and low-polymerized over-stoichiometric (preferentially molecular-type) g-$As_{55}Se_{45}$, using multifrequency temperature-modulated DSC-TOPEM® complemented with microstructure research based on Raman scattering (RS) microspectroscopy.

It is shown that high-polymerized network composed of $AsSe_3$ pyramidal fragments interlinked by long Se chains with small number of Se_8 molecular units (decoupled from this network under melt quenching) prevails in both melt-quenched and nanomilling-derived g-As_5Se_{95} samples. Transition to more polymerized network occurs in this glass under nanostructurization by nanomilling, being caused by incorporation of destroyed Se_8 molecules into the glass backbone. As a result, nanostructurization-driven calorimetric

response in this glass dominates with the known effect of size-induced glass-transition temperature depression.

The low polymerized preferentially molecular-type structure of g-$As_{55}Se_{45}$ is built of arsenoselenide network enriched with tetra-arsenic selenide molecules decoupled from this network under melt quenching. Molecular-to-network transition owing to nanomilling-driven destruction of the above molecular units and their incorporation into newly polymerized glass-forming backbone occurs in this glass undergoing nanostructurization, thus resulting in strong increase in calorimetric glass-transition temperature.

Acknowledgements The paper is a part of scientific research within the project No 0122U001806, the subject of Scientific Program funded by Ministry of Education and Science of Ukraine for years 2022–2024.

Declarations

Conflict of interest On behalf of all co-authors, the corresponding author states that there is no conflict of interest.

References

1. Roduner E. Nanoscopic materials. Size-dependent phenomena. Cambridge: RSC Publication; 2006.
2. Naterer GF. Heat transfer in single and multiphase systems. Boca Raton, London, New York, Washington: CRC Press LLC; 2003.
3. Roduner E. Size matters: why nanomaterials are different. Chem Soc Rev. 2006;35:583–92. https://doi.org/10.1039/B502142C.
4. Qadri SB, Skelton EF, Hsu D, Dinsmore AD, Yang J, Gray HF, Ratna BR. Size-induced transition-temperature reduction in nanoparticles of ZnS. Phys Rev B. 1999;60:9191–3. https://doi.org/10.1103/PhysRevB.60.9191.
5. Tomaszewski PE. Phase transitions in extremely small crystals. Ferroelectrics. 2008;375:74–91. https://doi.org/10.1080/00150190802437910.
6. Gilbert B, Zhang H, Feng H, Finnegan MP, Waychunas GA, Banfield JF. Special phase transformation and crystal growth pathways observed in nanoparticles. Geochem Trans. 2003;4:20–7. https://doi.org/10.1039/b309073f.
7. Prabhu D, Narayanasamy A, Shinoda K, Jeyadeven B, Greneche J-M, Chattopadhyay K. Grain size effect on the phase transformation temperature of nanostructured $CuFe_2O_4$. J Appl Phys. 2011;109:013532-1–6. https://doi.org/10.1063/1.3493244.
8. Reiter G. Mobility of polymers in films thinner than their unperturbed size. Eur Lett. 1993;23:579–84. https://doi.org/10.1209/0295-5075/23/8/007.
9. Keddie JL, Jones RA, Cory RA. Size-dependent depression of the glass transition temperature in polymer films. Eur Lett. 1994;27:59–64. https://doi.org/10.1209/0295-5075/27/1/011.
10. Keddie JL, Jones RAL, Cory RA. Interface and surface effects on the glass-transition temperature in thin polymer films. Faeaday Discuss. 1994;98:219–30. https://doi.org/10.1039/FD9949800219.
11. Keddie JL, Jones RA. Glass transition behavior in ultra-thin polystyrene films. Isr J Chem. 1995;35:21–6. https://doi.org/10.1002/ijch.199500005.
12. Cangialosi D, Alegria A, Colmenero J. Effect of nanostructure on the thermal glass transition and physical aging in polymer materials. Progr Polym Sci. 2016;54–55:128–47. https://doi.org/10.1016/j.progpolymsci.2015.10.005.
13. Feltz A. Amorphous inorganic materials and glasses. Weinheim: VCH; 1993.
14. Tanaka K, Shimakawa K. Amorphous chalcogenide semiconductors and related materials. New York, Dordrecht, Heidelberg, London: Springer; 2011.
15. Feltz A, Aust H, Blayer A. Glass formation and properties of chalcogenide systems XXVI: permittivity and the structure of glasses As_xSe_{1-x} and Ge_xSe_{1-x}. J Non-Cryst Solids. 1983;55:179–90. https://doi.org/10.1016/0022-3093(83)90667-1.
16. Yang G, Bureau B, Rouxel T, Gueguen Y, Gulbiten O, Roiland C, Soignard E, Yarger JL, Troles J, Sangleboeuf J-CH, Lucas P. Correlation between structure and physical properties of chalcogenide glasses in the As_xSe_{1-x} system. Phys Rev B. 2010;82:195206-1–8. https://doi.org/10.1103/PhysRevB.82.195206.
17. Shpotyuk O, Kozdras A, Baláz P, Bujnáková Z, Shpotyuk Y. Thermal-alteration interphase transformations in natural and synthetic arsenic sulfide polymorphs. J Chem Thermodyn. 2019;128:110–8. https://doi.org/10.1016/j.jct.2018.08.019.
18. Shpotyuk O, Kozdras A, Balaz P, Bujnakova Z, Shpotyuk Y. DSC TOPEM study of high-energy mechanical milling-driven amorphization in β-As_4S_4-based arsenicals. J Therm Anal Calorim. 2019;135:2935–41. https://doi.org/10.1007/s10973-018-7613-0.
19. Shpotyuk Y, Demchenko P, Bujňáková Z, Baláž P, Boussard-Pledel C, Bureau B, Shpotyuk O. Effect of high-energy mechanical milling on the medium-range ordering in glassy As-Se. J Am Ceram Soc. 2020;103:1631–46. https://doi.org/10.1111/jace.16877.
20. Shpotyuk Y, Demchenko P, Shpotyuk O, Balitska V, Boussard-Pledel C, Bureau B, Lukáčová Bujňáková Z, Baláž P. High-energy mechanical milling-driven *reamorphization* in glassy arsenic monoselenide g-AsSe: on the path tailoring special molecular-network glasses. Materials. 2021;14:44781-1–4. https://doi.org/10.3390/ma14164478.
21. Lucas P, Coleman GJ, Sen S, Gui S, Guimond Y, Calvez L, Boussard-Pledel C, Bureau B, Troles J. Structural and chemical homogeneity of chalcogenide glass prepared by melt-rocking. J Chem Phys. 2019;150:014505-1–9. https://doi.org/10.1063/1.5054704.
22. Ravindren S, Gunasekera K, Tucker Z, Diebold A, Boolchand P, Micoulaut M. Crucial effect of melt homogenization on the fragility of non-stoichiometric chalcogenides. J Chem Phys. 2014;140:134501-1–9. https://doi.org/10.1063/1.4869107.
23. Fraga I, Montserrat S, Hutchinson J. TOPEM, a new temperature modulated DSC technique. Application to the glass transition of polymers. J Therm Anal Calorim. 2007;87:119–24. https://doi.org/10.1007/s10973-006-7969-4.
24. Pielichowska K, Krol P, Krol B, Pagacz J. TOPEM DSC study of glass transition region of polyurethane cationomers. Thermochim Acta. 2012;545:187–93. https://doi.org/10.1016/j.tca.2012.06.029.
25. Gabbott P. Chapter 1: a practical introduction to differential scanning calorimetry. In: Paul G, editor. Principles and applications of

thermal analysis. Oxford, Ames, Carltoon: Blackwell Publ. Ltd; 2008. p. 1–50. https://doi.org/10.1002/9780470697702.
26. Kovanda V, Vlcek M, Jain H. Structure of As-Se and As-P-Se glasses studied by Raman spectroscopy. J Non-Cryst Solids. 2003;326&327:88–92. https://doi.org/10.1016/S0022-3093(03)00383-1.
27. Golovchak R, Oelgoetz J, Vlcek M, Esposito A, Saiter A, Saiter J-M, Jain H. Complex structural rearrangements in As-Se glasses. J Chem Phys. 2014;140:054505-1–8. https://doi.org/10.1063/1.4863561.
28. Saiter JM. Physical ageing in chalcogenide glasses. J Optoelectron Adv Mater. 2001;3:685–94.
29. Shpotyuk O, Golovchak R, Kozdras A. Physical ageing of chalcogenide glasses. In: Chalcogenide glasses: preparation, properties and applications. Philadelphia, New Delhi: Woodhead Publ.; 2014. p. 209–64. https://doi.org/10.1533/9780857093561.1.209.
30. Lucovsky G. Optic modes in amorphous As_2S_3 and As_2Se_3. Phys Rev B. 1972;6:1480–9. https://doi.org/10.1103/PhysRevB.6.1480.
31. Yannopoulos SN, Andrikopoulos KS. Raman scattering study on structural and dynamical features of noncrystalline selenium. J Chem Phys. 2004;121:4747–58. https://doi.org/10.1063/1.1780151.
32. Lucovsky G, Mooradian A, Taylor W, Wright GB, Keezer RC. Identification of the fundamental vibrational modes of trigonal, α-monoclinic and amorphous selenium. Solid State Commun. 1967;5:113–7. https://doi.org/10.1016/0038-1098(67)90006-3.
33. Lannin JS. Raman scattering properties of amorphous As and Sb. Phys Rev B. 1977;15:3863–71. https://doi.org/10.1103/PhysRevB.15.3863.
34. Ystenes M, Menzel F, Brockner W. *Ab initio* quantum mechanical calculations of energy, geometry, vibrational frequencies and IR intensities of tetraphosphorus tetrasulphide, α-P_4S_4 (D_{2d}), and vibrational analysis of As_4S_4 and As_4Se_4. Spectrochim Acta. 1994;50A:225–31. https://doi.org/10.1016/0584-8539(94)80050-2.
35. Ystenes M, Brockner W, Menzel F. Scaled quantum mechanical (SQM) calculations and vibrational analyses of the cage-like molecules P_4S_3, As_4Se_3, P_4Se_3, As_4S_3, and PAs_3S_3. Vib Spectrosc. 1993;5:195–204. https://doi.org/10.1016/0924-2031(93)87068-5.